CrossMark

Heliospheric Effect on Solar Activity Parameters during Maximum Phase of Solar Cycle 24 (2012–2015)

P. R. Singh[1] , Upendra Kr. Singh Kushwaha[1], A. K. Singh[2] , and T. K. Pant[3]
[1] Department of Physics, University of Allahabad, Prayagraj 211003, India; prithvisingh77@gmail.com
[2] Department of Physics, Banaras Hindu University, Varanasi 221005, India
[3] Space Physics Laboratory, VSSC, Thiruvananthapuram 695022, India

Abstract

The time series of daily data on solar activity proxies, namely the sunspot number (SSN), sunspot area (SSA), solar radio flux (F10.7), modified coronal index (MCI), solar flare index (FI), and cosmic ray intensity (CRI), were analyzed to understand the solar activity modulations and short-term periodicities therein. Rieger-type and other short-term periods include the solar rotational period that covers the maximum activity phase period (maximum phase of solar cycle 24). The wavelet power spectra and Periodogram of SSN, SSA, F10.7, MCI, FI, and CRI exhibited a significant short-term period. The heliospheric effects exist for a particular period ($\sim$27 days) and they are related to the solar activity phenomena. The cross-correlation coefficients and time lags between the CRI and solar activity parameters were estimated to be $\sim$200, 46, 281, 39, and 47 days for SSN, SSA, F10.7, MCI, and FI respectively during the time series 2012–2015 (maximum phase of solar cycle 24).

Key words: Sun: activity – Sun: flares – Sun: heliosphere – Sun: rotation – (Sun:) sunspots

1. Introduction

The variation of solar activity has important phenomena for understanding the solar internal structure, solar-terrestrial relationships, and global changes in the Earth's climate system. Coronal mass ejections (CMEs), solar flares, and coronal holes produce a disturbance in the interplanetary medium through a Forbush decrease (FD; Singh et al. 2010). A modulation of an interplanetary magnetic field (IMF), solar wind, and galactic cosmic ray flux are manifested in the heliospheric space environment (Chowdhury et al. 2016; Singh et al. 2018, 2021c, and references therein). The solar activity variations in each solar cycle are not constant because cosmic ray modulation varies (Chowdhury et al. 2010, 2016; Potgieter 2013; Singh et al. 2019, 2021a; De Oliveira et al. 2020 and references therein).

The variations in cosmic ray intensity (CRI) are physically related to high-speed streams from coronal holes and anti-phase variations with solar activity. The variation in galactic cosmic rays (GCRs) has been considered an effective probe for space weather. The joint processes of differential rotation and turbulent solar magnetic fields are directly related to the GCRs (Gil & Alania 2013). When entering the heliosphere, GCRs experience turbulent solar winds with an associated IMF, which contributes to major temporal and global variations in their energy and strength. This mechanism is known as solar modulation of GCRs.

Sierra-Porta (2018) reported the relationship between daily CRI with sunspot numbers (SSNs) and flare index (FI) for three solar cycles 21–23 and found a correlation over 0.85 and 0.75 with a time lag of 181 and 156 days respectively. Singh et al. (2018) reported that the time lag between solar flares and CRI is 4 and 12 months and that for coronal index and CRI is 3 and 10 months for solar cycles 22 and 23, respectively. Singh et al. (2022) observed a heliospheric effect on the descending phase of sunspot area (SSA) with GCRs (Moscow) during solar cycles 22, 23, and 24 of 5, 12, and 4 months respectively.

Solar activity exhibits a wide range of periodicities of $\sim$11 yr and intermediate-terms between the periods of $\sim$27 days and $\sim$11 yr. Intermediate-term periodicities are used to understand the mechanisms of solar variability and the solar-terrestrial relationship (Chowdhury et al. 2013, 2016; Singh et al. 2019, 2021b and references therein). The intermediate-terms and short-term periods, including the Rieger-type for various solar activity parameters, have been reported by various researchers (Lara et al. 2008; Lobzin et al. 2012; Singh et al. 2012; Chowdhury et al. 2013; Singh et al. 2021c, 2023 and references therein). Chowdhury et al. (2016) reported Rieger-type periods of GCR data during solar cycle 24 in the length of $\sim$130–170 days from the middle of 2011 to the middle of 2012. Kudela et al. (1991) reported two distinct CRI periods: long-term and intermediate-term. These periods are established by solar activity dynamics and transient effects in interplanetary space. Short-term periods, including $\sim$27 days and Rieger-type periods, have been observed in GCRs for different solar cycles (Mavromichalaki et al. 2003; Kudela et al. 2010; Gil & Alania 2012; Singh et al. 2021c; Singh & Singh Kushwaha 2024).

The main aim of this study is to investigate the short-term period and their behavior over the maximum phase of solar cycle 24. In addition, we study the heliospheric effect for a particular period of ∼27 days during the time series 2012–2015 (maximum phase of solar cycle 24).

2. Data and Analysis Methods

2.1. Datasets

In this study, we used daily data in time series from 2012 January to 2015 December (covering the solar maximum of solar cycle 24), i.e., a 4 yr data set of various solar activity parameters including SSN, SSA, solar radio flux (F10.7), modified coronal index (MCI), solar FI, and CRI. The daily data on SSN are taken from the World Data Centre (WDC-SILSO, Royal Observatory of Belgium, Brussels) from https://www.sidc.be/SILSO/datafiles. The daily data of the SSA are taken from http://solarcyclescience.com/AR~Database/daily~area.txt. Daily data of the MCI are taken from https://www.kozmos-online.sk/slnko/modifikovany-koronalny-index-modified-coronal-index/. The daily data of the solar FI are taken from http://www.koeri.boun.edu.tr/astronomy/fi~nedir.htm. The daily data of F10.7 are taken from https://spaceweather.gc.ca/forecast-prevision/solar-solaire/solarflux/sx-5-en.php. For CRI data, we have considered the low cutoff rigidity neutron monitor McMurdo (MCMU) station which is situated at McMurdo (Latitude: 77.90o S Longitude: 166.60o E, Cutoff Rigidity: 0.0 GV), Antarctica, and run by the Bartol Institute and has been in continuous operation since 1964. The daily pressure–corrected CRI data are taken from http://cr0.izmiran.ru/mcmd/main.htm.

2.2. Analysis Methods

To observe the short-term period of solar activity parameters (SSN, SSA, F10.7, MCI, and FI) and CRI during the maximum phase of solar cycle 24 (2012–2015), we used three different methods: (1) fast Fourier transform (FFT), (2) R RobPer method, and (3) Morlet wavelet power spectra methods, to find short-term periods. In addition, the R package RobPer analysis employing the least squares regression technique (L2 model) was used for periodicity estimation (Thieler et al. 2013; Wang 2013; Thieler et al. 2016; Singh et al. 2021a, 2023, Singh & Singh Kushwaha 2024).

2.3. Cross–Correlation Analysis

Cross–correlation analysis (CCA) is a commonly applied method for determining the phase relation between different solar activities. We calculated the value of cross-correlation between solar activity (SSN, SSA, F10.7, MCI, and FI) with CRI using this equation

$$CC(C/S) = \frac{\sum_{i=1}^{n}[C(i) - \bar{C}][S(i + \triangle) - \bar{S}]}{(n-1)\sigma_C \sigma_S}, \qquad (1)$$

where $\bar{C}$ and $\bar{S}$ represent the mean values of CRI and solar activity (SSN, MCI, and FI), respectively, while σ_C and σ_S are their corresponding standard deviations and $\triangle$ is the delay time.

3. Result and Discussion

Solar cycle 24 started in 2008 December and entered the maximum phase from 2012 to 2015, i.e., a 4 yr data set. The Sun exhibited high solar activity during the maximum phase of cycle 24. Figure 1(a)–(f) shows the daily data variation of SSN, SSA, F10.7, MCI, FI, and CRI for the study period. The daily data of SSN, SSA, F10.7, and MCI feature a maximum and minimum pattern, and a plateau during the study period in Figure 1(c), (d), (e), and (f). A different trend (variation) has been detected in the FI in Figure 1(b). SSN, SSA, F10.7, FI, and MCI show a prominent peak in the early phase of 2014, (i.e., solar cycle 24 is a maximum phase during 2014). The peak value of solar activity during 2014 for SSN is 207, SSA is 4326, F10.7 is 262, MCI is 3.07, and FI is 171.58. The daily data of the CRI gradually decrease from 2012 to 2015. The daily data value of CRI is also a plateau type in Figure 1(a). In this study period, CRI manifests an anti-phase relationship between solar activity parameters (SSN, SSA, MCI, FI, and F10.7).

This study used a mixed-phase polarity field $A < 0$ (2012 to the middle of 2013) and $A > 0$ (middle of 2013–2015). The orientation of the field (polarity) is defined as a positive polarity field, denoted as $A > 0$, and a negative field, denoted as $A < 0$ (Chowdhury et al. 2016). Pesnell (2014) and Singh et al. (2021a) reported that the amplitude of solar cycle 24 was weaker than that in solar cycle 23. Richardson (2013) reported that solar cycle 24 is likely to be the weakest cycle on the grounds of low geomagnetic activity in the first four years of the rising phase of solar cycle 24. We know that solar cycle 24 was distinguished by its lower activity in comparison with the previous solar cycle because it is associated with fewer solar events that could cause great FDs. Li et al. (2016) reported a statistical relationship between SSN and SSA for the studied period from 1874 May to 2015 April. They have reported that the probability distribution of SSA generally decreases monotonically, however the distribution of SSN increases first, but decreases as a whole. They have also reported that the quadratic fit and linear fit of SSN and SSA are statistically significant as well as having a proportional relationship between them.

3.1. Periodicity of Solar Activity Parameters by R RobPer Method

From the R RobPer method, the periodic variation of SSN, SSA, F10.7, MCI, FI, and CRI in Figure 2(a)–(f) shows a significant short-term period for the data range between 10 and 600 days. The R RobPer periodogram of SSN, SSA, F10.7, MCI, FI, and CRI shows a significant solar rotational period is ∼26 days for all the values. We also observed a significant
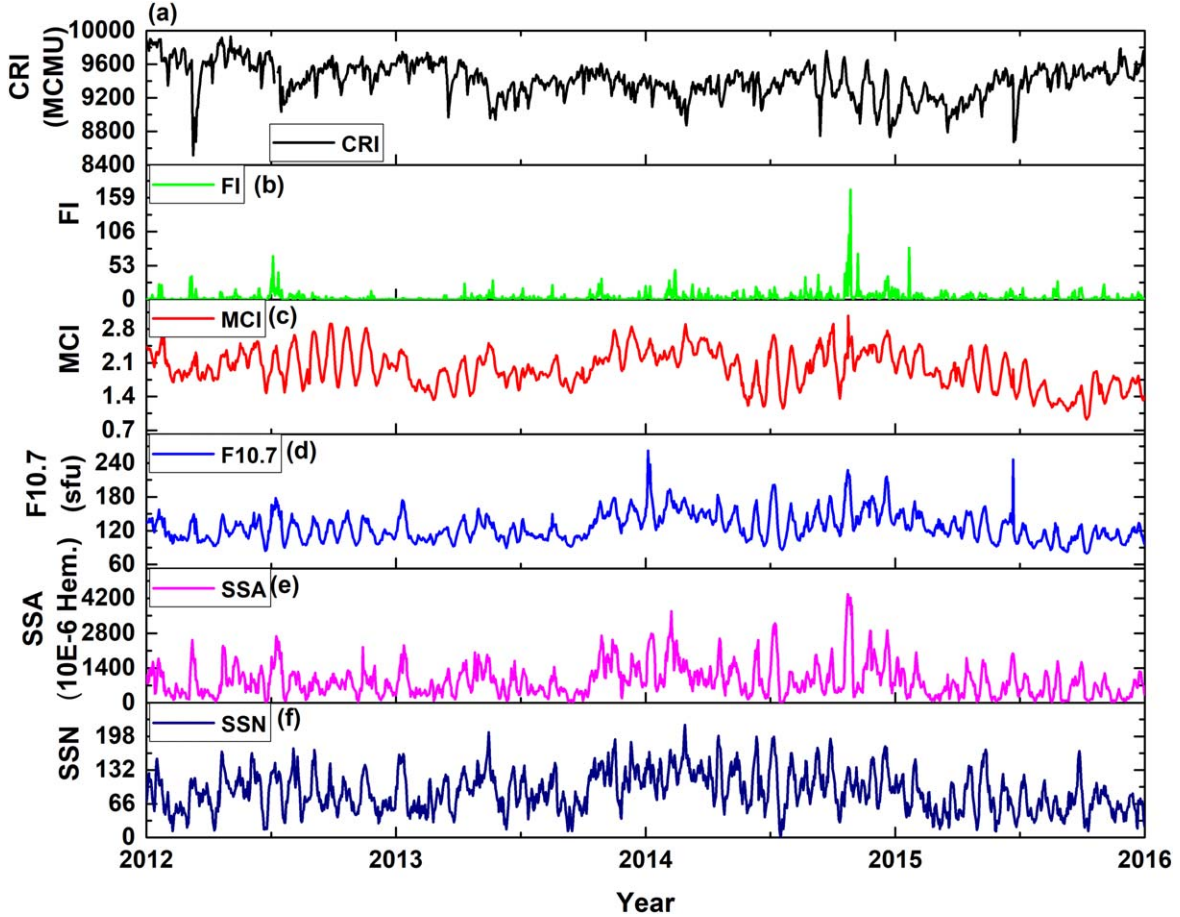
Figure 1. Time profiles of daily data variation for (a) CRI of neutron monitor station, (b) solar FI, (c) MCI, (d) F10.7, (e) SSA and (f) SSN during (2012–2015).

period (Rieger-type period) for SSN is ∼124 days, ∼139 days, ∼179 days, SSA is ∼148 days, ∼183 days, F10.7 is ∼179 days, MCI is ∼137 days, ∼183 days, FI is ∼143 days, ∼172 days and CRI is ∼120 days, ∼141 days and 162 days. We found a significant short-term period for SSN, SSA, F10.7, MCI, FI, and CRI is ∼274, ∼277, ∼266, ∼247, ∼283, and ∼316 days respectively. In addition, other significant short-term periods are indicated in Table 1. From Table 1: the SSN and MCI exhibited a significant common period of ∼135 days. This is probably the 5th harmonic of ∼27 days and as well CRI is the 6th harmonic of ∼27 days. SSN, SSA, and FI exhibit a significant period of ∼53 days, also representing the 2nd harmonic of ∼27 days. The SSA and MCI exhibited significant periods of ∼183 days, representing the 7th harmonic of ∼27 days. It is also well known as the Rieger-type period during the maximum phase of solar cycle 24 (2012–2015).

3.2. Periodicity of Solar Activity by FFT Method

The physical frequency is the distinction between a Rieger-type period and solar rotational periods of ∼27 days. The physical frequency is almost at a higher peak in the periodogram of FFT. We detected short-term periods in the range of 10–600 days using the FFT method. The Rieger-type periodicity is most prominent during the study time series of 2012–2015. The periodic variation of solar activity parameters, such as SSN, SSA, F10.7, MCI, FI, and CRI, is depicted in Figure 3(a)–(f). In the FFT method, we used the 1σ standard deviation value (67.87%) significant power in all solar activity parameters, as indicated by the red dotted line in Figure 3(a)–(f).

The FFT periodogram of SSN, SSA, F10.7, MCI, FI, and CRI in Figure 3 exhibits a significant solar rotational period of ∼26 days. The other significant periods such as (the Rieger-type period) for SSN is ∼146 days and ∼182 days, SSA is ∼146 days and ∼182 days, F10.7 is ∼182 days, MCI is ∼132 days and ∼182 days, FI is ∼121 days and ∼146 days, and CRI is ∼121 days and ∼146 days. The significant short-term period for SSN, SSA, FI, and CRI is ∼292 days but for F10.7 it is ∼365 days and MCI it is ∼243 days. In addition, other significant periods are indicated in Table 1. From Table 1: the SSN, SSA, and FI exhibit a significant period of ∼58 days, also
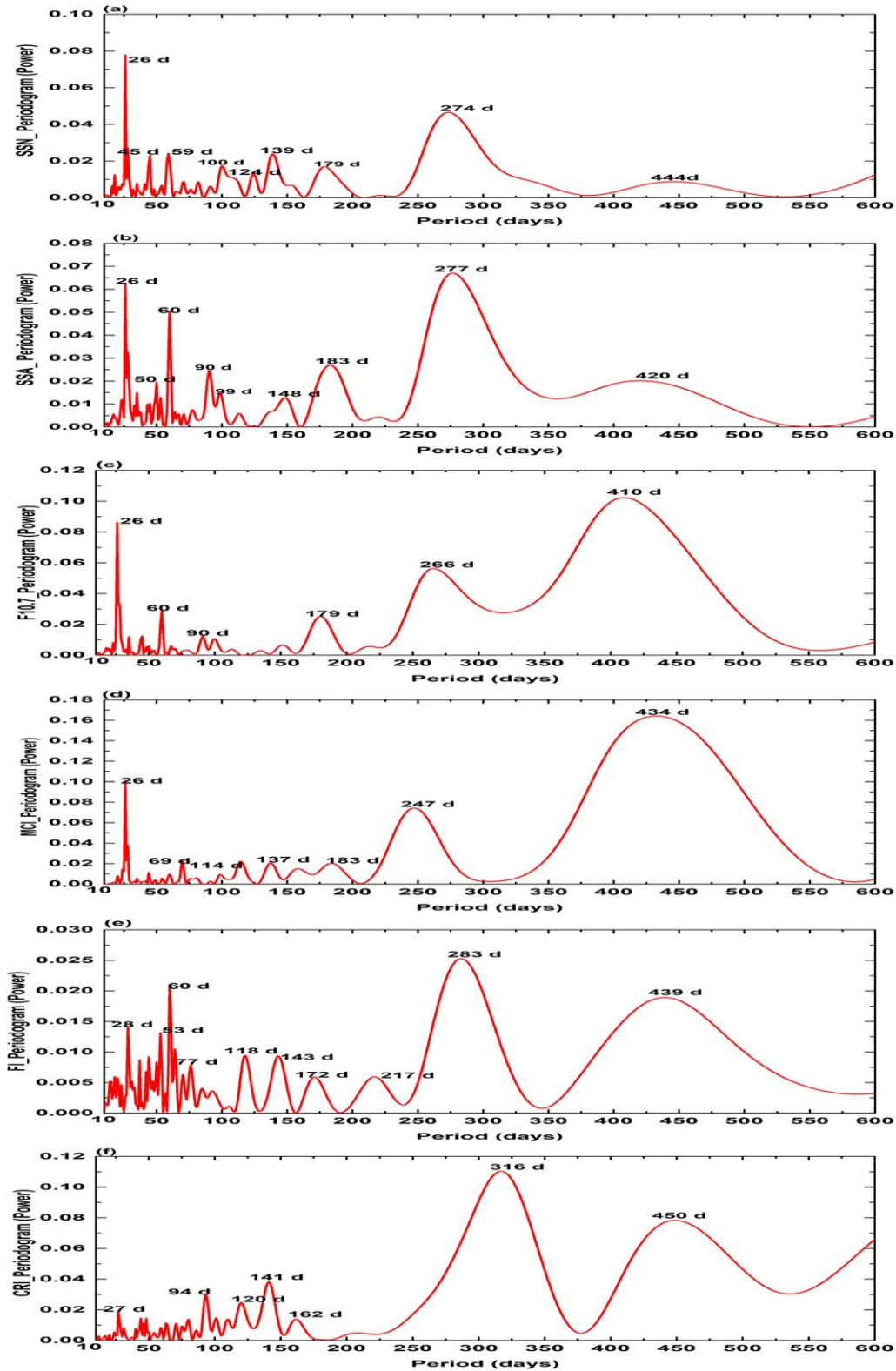
Figure 2. Short-term periods of (a) SSN, (b) SSA, (c) F10.7, (d) MCI, (e) FI, and (f) CRI (MCMU) by R RobPer Method during maximum phase of solar cycle 24 and data range (10–600 days).

Table 1
The Significant Periods' Value of Solar Activity Parameters (SSN, MCI, SSA, F10.7, and FI) and CRI (MCMU) by Two Different Methods During the Maximum Phase of Solar Cycle 24 (2012–2015)

Solar Activity Indicator	FFT Methods (in days)	R RobPer Methods (in days)
SSN	∼292, 182, 146, 104, 58, 44, 26	∼274, 179, 139, 124, 100, 59, 45, 26
SSA	∼292, 182, 146, 91, 60, 50, 34, 26	∼277, 183, 148, 99, 90, 60, 50, 26
F10.7	∼365, 182, 91, 60, 44, 34, 26	∼266, 179, 90, 60, 26
MCI	∼243, 182, 132, 112, 69, 26	∼247, 183, 137, 114, 69, 26
FI	∼292, 146, 121, 76, 60, 52, 44, 34, 28	∼283, 217, 172, 143, 118, 77, 60, 53, 28
CRI	∼292, 146, 121, 91, 44, 28	∼316, 162, 141, 120, 94, 27

representing the 2nd harmonic of ∼27 days. The most significant short-term period of ∼292 days is present for the FFT periodograms of SSN, SSA, FI, and CRI. It is the 11th harmonic of approximately ∼27 days.

From Table 1, we established a comparative study for the variation of significant period value of solar activity parameters by two different periodogram methods (FFT and R RobPer). The periodogram of solar activity parameters for significant periods is approximately similar by both of the methods R RobPer and FFT. These two methods are strongly related to each other. These periods depend on the solar activity variation from equator to pole, as well as the rotation of the Sun. The above short-term periods are related to the solar rotation of the Sun.

3.3. Wavelet Power Spectra of Solar Parameters

The wavelet power spectra of SSN, SSA, F10.7, MCI, FI, and CRI are presented in short-term and Rieger-type periods by the Morlet wavelet method, as shown in Figure 4(a)–(f). The thin black contours represent the wavelet power spectra above the 95% confidence level. The left panels of Figure 4(a)–(f), represent wavelet power spectra of SSN, SSA, F10.7, MCI, FI, and CRI during the maximum phase of solar cycle 24 (2012–2015), i.e., 4 yr data set, from top to bottom respectively. From Table 2, we found a significant contour as a short-term period with different time spans for SSN, F10.7, and CRI is ∼23–27 days, and for SSN, SSA, F10.7, MCI, and FI the time span is ∼27 days, with the time span as indicated in Table 2. The short-term period for SSN, SSA, and F10.7 is ∼263 days, for CRI it is ∼179–263 days, for MCI it is ∼221 days, and for FI it is ∼302 days, with the time span as indicated in Table 2. Some other significant contours corresponding to short-term periods are indicated in Table 2.

The global wavelet power spectrum is shown in Figure 4(a)–(f) in the right panel. We found a significant solar rotational period of ∼27 days for SSN, SSA, F10.7, and MCI. The short-term period is present and dominating in the global wavelet spectra with a period of ∼314 days, and it is statistically significant for SSA, FI, and CRI, but for SSN and MCI is ∼264 days and for F10.7 is ∼374 days. Some other significant short-term periods for SSN are

∼111 days, SSA is ∼93 days, FI is ∼55 days, and CRI is ∼132 days (Rieger-type).

Bai & Sturrock (1991) reported that the periodicity of solar flares was ∼84 days and ∼127 days during solar cycle 20. Kilcik et al. (2010) observed a significant period in the FI of ∼115 days during cycle 23. Bai (1992) observed the relative periodicities for solar activity parameters of solar flares and SSAs, such as ∼128, ∼102, ∼78, and ∼51 days. Bai (2003) reported that the period of solar flare occurrence during the ascending phase of cycle 23 was ∼33.5 days. Oliver & Ballester (1995) and Chowdhury et al. (2009) observed significant periods of ∼41, ∼74, ∼77, ∼83, ∼87, and ∼106 days for solar flare and SSAs during solar cycle 22. The existence of Rieger-type periods in SSNs during solar cycle 23 has been reported (Chowdhury & Dwivedi 2011; Singh & Badruddin 2014). Chowdhury et al. (2014) reported that the significant short-term periodicities for SSN and SSA are ∼43, ∼45, ∼53, and ∼60 days using the Lomb-Scargle (L-S) method (Lomb-Scargle periodogram) during the ascending phase of solar cycle 24. It is also indicated by the L-S power spectrum exhibiting significant solar rotational period of ∼27 days along with ∼114 days, and Rieger-type period of ∼142 and ∼189 days. The wavelet spectrum of SSN and SSA exhibits a highly significant period of ∼213 days and ∼32 days between January 2011 and around the middle of 2013. The other period is ∼130 days from the end of 2012 to mid-2013, but it is out of the cone of influence and there are significant Rieger-type periods between ∼160 and ∼220 days from the middle of 2010 to the end of 2012.

Jayalekshmi et al. (2022) observed short-term significant periods of SSNs ∼25, ∼28, ∼30,∼33, ∼38, ∼46, and ∼61 days during the time span 1819–2019. Recently, Kilcik et al. (2024) reported that the period of ∼25–33 days for daily data of cosmic rays, solar FI, and coronal index during solar cycle 24 (2008 December–2019 December) by using methods of the Morlet wavelet, cross-wavelet, and multi-taper. It is also reported that other periods for FI,CI and CRI are ∼52–61 day. Caballero & Valdés-Galicia (2001) reported that the GCR periods were ∼40, ∼55, and ∼78 days during the ascending phase of solar cycle 23 and the declining phase of solar cycle 22. GCRs also exhibit Rieger-type periods of
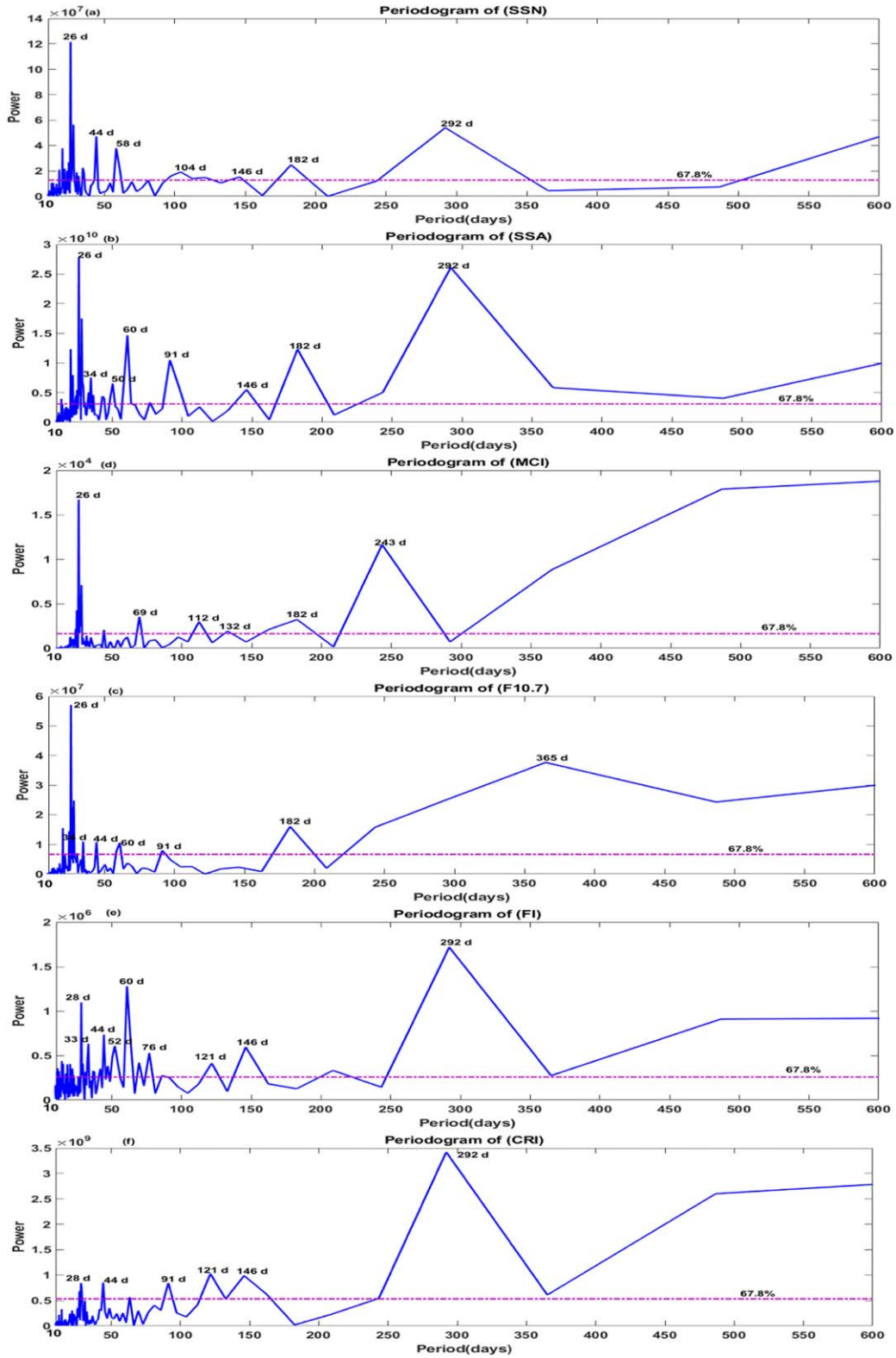
Figure 3. Short-term period of (a) SSN, (b) SSA, (c) F10.7, (d) MCI, (e) FI, and (f) CRI (MCMU) by FFT method during maximum phase of solar cycle 24 and data range (10–600 days).
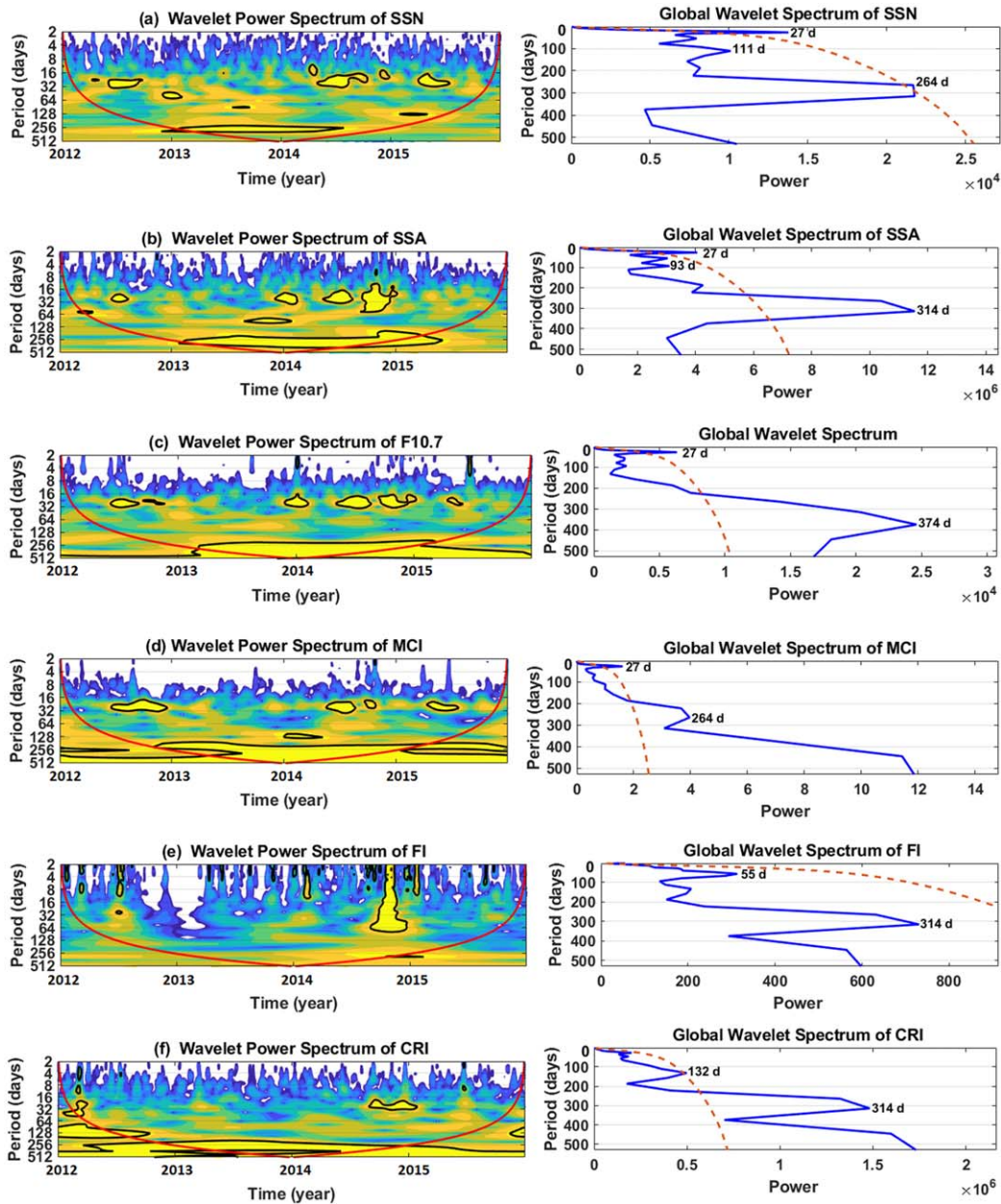
Figure 4. Short-term periods of (a) SSN, (b) SSA, (c) F10.7, (d) MCI, (e) FI, and (f) CRI (MCMU) by Morlet wavelet power spectra (left panels) and global wavelet spectra (right panels) during maximum phase of solar cycle 24 (2012–2015).

∼130–180 days (Vecchio et al. 2010; Sabbah & Kudela 2011; Gil & Alania 2012; Laurenza et al. 2012; Modzelewska & Alania 2013; Chowdhury et al. 2016, and references therein).

Deng et al. (2020) reported the solar rotational period (∼27.5 days) for the MCI is significant during the study period from 1939 January 1, to 2019 May 31, by using continuous wavelet transform methods. It is also reported that other significant periods are 38, and 128 days. They also reported a phase relationship between solar magnetic activity and the coronal

rotation period. Zhang et al. (2023) observed the temporal variation of solar rotation in the transition region for the photosphere, chromosphere, and corona by using Lyα irradiance from 1947 February 14 to 2023 February 20. They found the sidereal rotational period is 25.50 days and the solar transition region varies between 22.24 and 31.49 days for the period of study.

We ascertained a significant period for SSN is ∼26, ∼140, and ∼292 days, during the maximum phase of solar cycle 24 by

Table 2
The Period Values of CRI (MCMU) and Solar Activity Parameters (SSN, MCI, SSA, F10.7, and FI) by Morlet Wavelet Methods During the Maximum Phase of Solar Cycle 24

Solar Activity Indicator	Wavelet Power Spectra Period (in days)	Time Span
...	~23-27	2014 Dec–Jun
...	~27	2012 Jun–Sep and 2014 May–Oct
SSN	~46	2012 Dec–2013 Jan
...	~131	2015 Feb–May
...	~263	2013 Feb–2014 July
...	~27	2012 Jun–Aug, 2013 Dec–2014 Feb, and 2014 May–Aug
SSA	~27-32	2014 Sep–Dec
...	~93	2013 Sep–2014 Jan
...	~263	2013 March–2015 May
...	~23-27	2014 Sep–Dec
F10.7	~27	2012 Jun–Aug, 2013 Dec–2014 Feb, and 2014 May–Aug
...	~263	March 2013–Nov 2014
MCI	~27	2012 Jun–Dec, 2014 May–Aug, and 2015 April–July
...	~221	2012 Nov–2015 Jun
...	~27	2012 Jun–July
FI	~55	2014 Sep–Dec
...	~302	2014 Oct–2015 Feb
...	~23–27	2014 Sep–2015 Jan
CRI	~110–131	2012 Jan–Sep
...	~179–263	2013 Jan–2014 Sep

different methods and it is in good agreement with Kilcik et al. (2024) and Jayalekshmi et al. (2022). The short-term periods depend on the motion of the Sun. The motion of the Sun is explained on the basis of dynamo theory. The nature of different periods is related to the dynamo theory of the Sun. Our analyses show the presence of a Rieger-type period and a harmonic of ∼27 days. The wavelet power spectrum, FFT, and R Robper method of daily data of solar activity parameters indicate a significant short-term period of ∼292 days. It is the 11th harmonic of ∼27 days. The wavelet power spectra show a pronounced period of ∼27 days for all solar activity parameters. Our FFT and R Robper results are consistent with the wavelet results.

3.4. Heliospheric Effect on Solar Activity

We study the heliospheric behavior of solar activity parameters during the maximum phase of solar cycle 24 (2012–2015) i.e., a 4 yr data set. In the heliospheric study, we used wavelet power spectral data for a specific period of ∼27 days. For this study, we used CCA and the time lags between CRI with solar activity parameters (SSN, SSA, F10.7, MCI, and FI). From Figure 5(a)–(e), we found that the heliospheric nature is present in solar activity parameters with CRI during the study period. From Table 3, we observed that the highest cross-correlation coefficient of CRI with SSN is 1.0 with a time lag of 200 days. Our study is reporting different kinds of results because we use a particularly significant period, ∼27 days of data for a fixed time, i.e., a four-year data set (maximum phase of solar cycle 24). During the solar maximum, the solar transients contribute to the modulation of solar activity. On the above results, the heliospheric nature is established. We conclude that the heliospheric effect is only related to the solar wind and depends on the strength of solar activity (depending on the extrasolar cosmic rays only near the Sun).

Many authors have studied time lags in various solar indices and have reported different time lags. Usoskin et al. (1998) reported the heliospheric nature of solar activity as transport of CRI modulation. The drift scenario of charged particle propagation enters the heliosphere region through the polar regions, and CRI enters the inner heliosphere through the equatorial region (Potgieter et al. 2001; Chowdhury et al. 2016). Aslam & Badruddin (2015) observed 90 and 600 day lags between international sunspot number (ISSN) and 10.7 cm solar radio flux with CRI. Mishra et al. (2006) reported 10 and 17 month time lags at two different neutron monitors (Oulu and Moscow neutron monitors) with ISSN. Chowdhury et al. (2016) observed the time lag between solar variables, such as SSN, SSA, CMEs, and MCI, with a GCR intensity of 10–17 months during the ascending phase of solar cycle 24. Tomassetti et al. (2017) observed a time lag of 8 months for ISSN with CRIs during the period 2000–2017.

Li et al. (2009) observed the phase synchronization between SSNs and SSAs in the time interval from 1874 November to 2007 September. They found a high level of phase synchronization between SSNs and SSAs around the minimum and maximum of a cycle (ascending and descending phases of cycles). Deng et al. (2012) investigated a phase asynchrony between SSN and coronal index with a phase lag of 30 days from 1939 January to 2008 December by using different methods like CWT, XWT, and WTC. They also reported the high-frequency components represent the asynchronous behavior of SSN and coronal index. Deng et al. (2013) reported a phase relationship between SSNs and 10.7 cm solar radio flux during the period of 1947 February–2012 June by using modern nonlinear tools. They reported the phase relationship between SSNs and 10.7 cm solar radio flux is frequency dependent. The 10.7 cm solar radio flux lags behind SSNs with relative phase differences being ∼3–4 months.
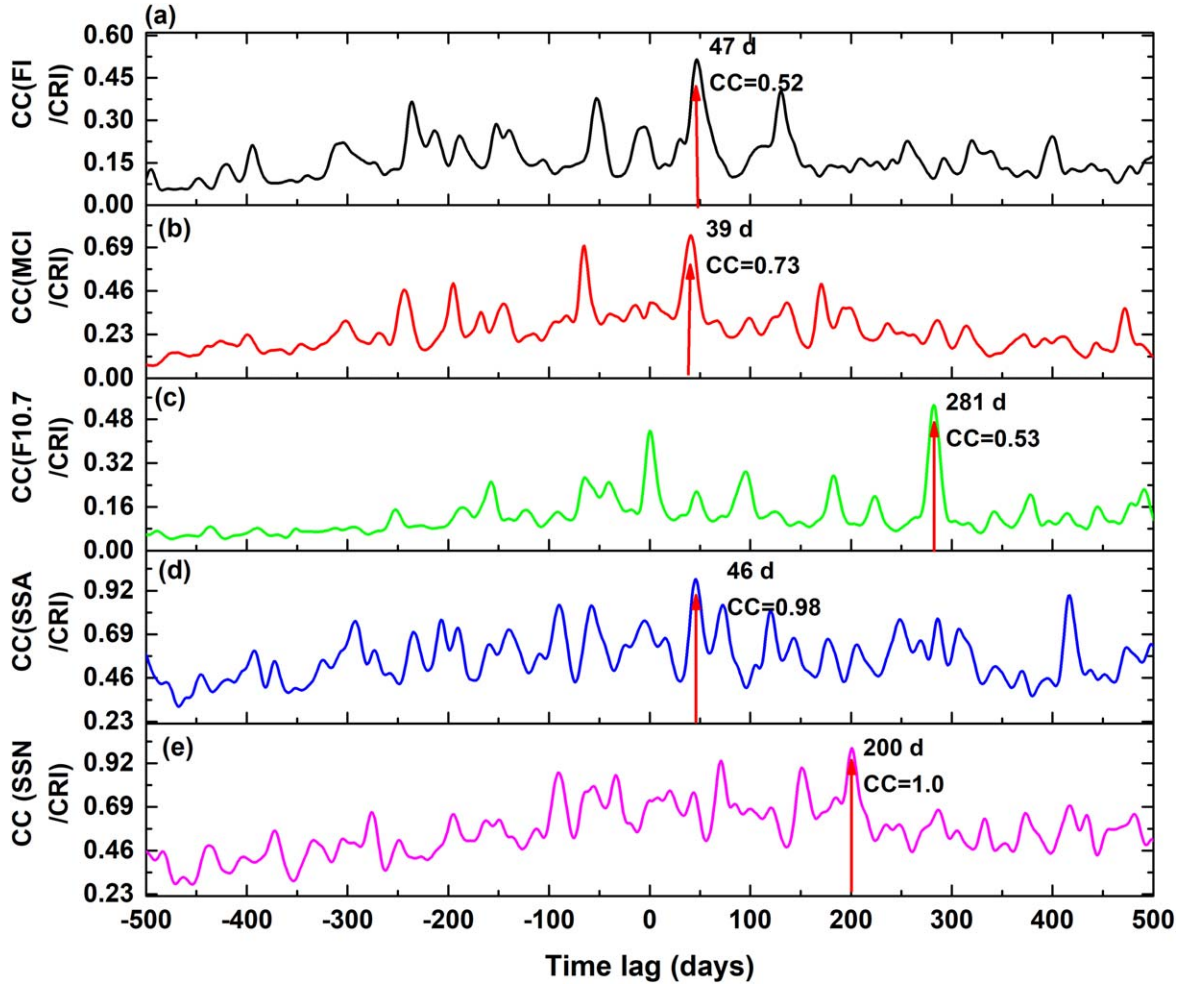
Figure 5. Cross correlations vs. time lag in days between CRI (MCMU) with (a) FI, (b) MCI, (c) F10.7, (d) SSA and (e) SSN, from top to bottom respectively. The vertical red lines correspond to maximum cross-correlation value during the maximum phase of solar cycle 24 (2012–2015).

Table 3
The Cross–Correlation Coefficients and the Corresponding Time Lags are Given for CRI (MCMU) with Solar Activity Parameters (SSN, SSA, F10.7, MCI, and FI)

Activity Indicator	Cross–Correction (CC)	Time Lags (in days)
SSN	1.0	200
SSA	0.98	46
F10.7	0.53	281
MCI	0.73	39
FI	0.52	47

4. Conclusion

The three different periodic analysis methods produce a short-term period for SSN, MCI, FI, SSA, F10.7, and CRI. In our study, we found two significant periods for SSN, FI, SSA, F10.7, and CRI as the 5th and 11th harmonics of ~27 days. We also found a common short-term period for all selected solar activity parameters is ~292 days. The periodic changes in different solar activity parameters are temporal due to the solar rotation of the Sun. Thus, the presence of solar rotational periods and Rieger-type periods is related to space weather. The dynamics of the solar interior and meridional circulation of the solar atmosphere are related to the short-term periods. The short-term period of the CRI is attributed to the configuration of the coronal holes and high-speed streams or heliospheric nature.

In this context, the CRI reveals a highly significant cross-correlation with the corresponding solar activity parameters (SSN, SSA, F10.7, MCI, and FI) with different time lags. The particular period of ~27 days of power spectral data shows a phase relation between CRI with SSN, MCI, FI, SSA, and F10.7, and they exhibit a heliospheric nature. The behavior of the heliospheric effect on the Earth is a joint process of solar magnetic activity. This study is more informative for understanding the Sun's physical properties as based on a heliospheric

nature and short-term periodic variation. The solar interior developed a periodic emergence of magnetic flux in the solar active region during the maximum phase of solar cycle 24.

Conflicts of Interest

The authors declare that there are no conflicts of interest.

ORCID iDs

P. R. Singh ⓘ https://orcid.org/0000-0003-3187-8812
A. K. Singh ⓘ https://orcid.org/0000-0002-8834-2464

References

Aslam, O. P. M., & Badruddin 2015, SoPh, 290, 2333
Bai, T. 1992, ApJ, 388, L69
Bai, T. 2003, ApJ, 591, 406
Bai, T., & Sturrock, P. A. 1991, Natur, 350, 141
Caballero, R., & Valdés-Galicia, J. F. 2001, AdSpR, 27, 583
Chowdhury, P., Choudhary, D. P., Gosain, S., & Moon, Y. J. 2014, Ap&SS, 356, 7
Chowdhury, P., & Dwivedi, B. N. 2011, SoPh, 270, 365
Chowdhury, P., Jain, R., & Awasthi, A. K. 2013, ApJ, 778, 28
Chowdhury, P., Khan, M., & Ray, P. C. 2009, MNRAS, 392, 1159
Chowdhury, P., Khan, M., & Ray, P. C. 2010, Ap&SS, 326, 191
Chowdhury, P., Kudela, K., & Moon, Y. J. 2016, SoPh, 291, 581
De Oliveira, M. N., Augusto, C. R. A., Navia, C. E., & Nepomuceno, A. A. 2020, arXiv:2003.06432v1
Deng, L. H., Li, B., Zheng, Y. F., & Cheng, X. M. 2013, NewA, 23, 1
Deng, L. H., Qu, Z. Q., Wang, K. R., & Li, X. B. 2012, AdSpR, 50, 1425
Deng, L. H., Zhang, X. J., Deng, H., Mei, Y., & Wang, F. 2020, MNRAS, 491, 848
Gil, A., & Alania, M. V. 2012, SoPh, 278, 447
Gil, A., & Alania, M. V. 2013, AdSpR, 52, 951
Jayalekshmi, G. L., Pant, T. K., & Prince, P. R. 2022, SoPh, 297, 85
Kilcik, A., Özgüç, A., Rozelot, J. P., & Ataç, T. 2010, SoPh, 264, 255
Kilcik, A., Rozelot, J. P., & Ozguc, A. 2024, Univ, 10, 107
Kudela, K., Ananth, A. G., & Venkatesan, D. 1991, JGR, 96, 15871
Kudela, K., Mavromichalaki, H., Papaioannou, A., & Gerontidou, M. 2010, SoPh, 266, 173
Lara, A., Borgazzi, A., Mendes, O., Jr+, Rosa, R. R., & Domingues, M. O. 2008, SoPh, 248, 155
Laurenza, M., Vecchio, A., Storini, M., & Carbone, V. 2012, ApJ, 749, 167
Li, K. J., Gao, P. X., & Zhan, L. S. 2009, SoPh, 255, 289
Li, K. J., Li, F. Y., Zhang, J., & Feng, W. 2016, SoPh, 291, 2917
Lobzin, V. V., Cairns, I. H., & Robinson, P. A. 2012, ApJ, 754, L28
Mavromichalaki, H., Preka-Papadema, P., Liritzis, I., Petropoulos, B., & Kurt, V. 2003, NewA, 8, 777
Mishra, A. P., Gupta, M., & Mishra, V. K. 2006, SoPh, 239, 475
Modzelewska, R., & Alania, M. V. 2013, SoPh, 286, 593
Oliver, R., & Ballester, J. L. 1995, SoPh, 156, 145
Pesnell, W. D. 2014, SoPh, 289, 2317
Potgieter, M. S. 2013, LRSP, 10, 1
Potgieter, M. S., Burger, R. A., & Ferreira, S. E. S. 2001, SSRv, 97, 295
Richardson, I. G. 2013, JSWSC, 3, A08
Sabbah, I., & Kudela, K. 2011, JGRA, 116, A04103
Sierra-Porta, D. 2018, Ap&SS, 363, 1
Singh, A. K., Siingh, D., & Singh, R. P. 2010, SGeo, 31, 581
Singh, P. R., Agrawal, S. L., Tiwari, C. M., & Singh, A. K. 2022, in 37th International Cosmic Ray Conf. (Trieste: SISSA), 1326
Singh, P. R., Farid, A. I. S., Pant, T. K., & Singh, A. K. 2021a, RAA, 21, 106
Singh, P. R., Farid, A. I. S., Singh, A. K., Pant, T. K., & Aly, A. A. 2021b, Ap&SS, 366, 48
Singh, P. R., Farid, A. I. S., Singh, Y. P., Singh, A. K., & Aly, A. A. 2021c, PhyS, 96, 125033
Singh, P. R., Saxena, A. K., & Tiwari, C. M. 2018, JApA, 39, 20
Singh, P. R., Singh, A. K., & Pant, T. K. 2023, JApA, 44, 14
Singh, P. R., & Singh Kushwaha, U. K. 2024, Ap&SS, 369, 78
Singh, P. R., Tiwari, C. M., Agrawal, S. L., & Pant, T. K. 2019, SoPh, 294, 118
Singh, Y. P., & Badruddin 2014, P&SS, 96, 120
Singh, Y. P., Gautam, S., & Badruddin 2012, JASTP, 89, 48
Thieler, A., Backes, M., Fried, R., & Rhode, W. 2013, SADM, 6, 73
Thieler, A. M., Fried, R., & Rathjens, J. 2016, JSS, 69, 1
Tomassetti, N., Orcinha, M., Barão, F., & Bertucci, B. 2017, ApJ, 849, L32
Usoskin, I. G., Kananen, H., Mursula, K., Tanskanen, P., & Kovaltsov, G. A. 1998, JGR, 103, 9567
Vecchio, A., Laurenza, M., Carbone, V., & Storini, M. 2010, ApJ, 709, L1
Wang, Z. 2013, JSS, 53, 1
Zhang, X., Deng, L., Fei, Y., Chun, L., & Tian, X. 2023, ApJ, 951, L3